INTERDISCIPLINARY DAMAGE AND STABILITY ANALYSIS OF A WIND TURBINE BLADE

Lars C.T. Overgaard and Erik Lund [Lars C.T. Overgaard]: lcto@ime.aau.dk
Department of Mechanical Engineering, Aalborg University
Pontoppidanstraede 101, DK-9220 Aalborg East, Denmark

Keywords: *Wind turbine blade; Instability; Mixed-mode cohesive element*

Abstract

A wind turbine blade is investigated based on full scale experiments, a geometrically nonlinear finite element analysis and a nonlinear fracture mechanics finite (NLFM) element model. In order to perform a NLFM analysis a mixed-mode de-cohesive element with a subplane solution strategy is implemented in the in-house finite element program MUST. Some performance benchmarks are shown and the implemented element and solution strategy perform well.

The formulation is employed on a section of a wind turbine blade and solved for this large three-dimensional structure. The material instability point is calculated together with the geometric instability point from the geometrically non-linear analysis. Both instability phenomena are found to coincide at almost the same load level, which indeed account for the progressive structural collapse seen in the full scale flap-wise experiment.

1 Introduction

When designing wind turbine blades a 50 year extreme gust wind profile decides the critical static flap-wise design load. Consequently, the suction side of the wind turbine blades, during operation and in qualification test, is loaded considerable in compression, which can trigger instability in the form of material and/or geometric instability. The interaction of both structural instabilities will reduce the overall strength of the blade and causes a progressive collapse of the structure.

The objective of this work is to predict the interdisciplinary effects of damage mechanics and stability analysis of a wind turbine blade section manufactured by Vestas Wind Systems A/S. For this purpose a continuum-based solid-shell element together with a mixed-mode de-cohesive element formulation is used. A geometrically nonlinear equivalent single layered shell finite element model is also used for analysis of the blade response.

The finite element models are evaluated and compared with full scale experiments of a 25-meter wind turbine blade.

On system level the blade is composed of a suction shell also called leeward side alias the compression flange and a pressure shell also called windward side alias the tension flange, see fig. 1(a). The flanges are the main contributors for moment of inertia in order to withstand flap-wise loading generated by the aerodynamical thrust from the wind. The web is typically a sandwich structure for withstanding shear force loading. The cord distance between the leading and trailing edges gives moment of inertia for the edge-wise loading primarily generated by the mass inertia of the blade during operations. The full scale experiment is in the flap-wise direction and therefore the main spar of the blade is the primary load-carrying structure.

On component level the main spar consists of a winding root, main and tip spar, upper and lower shell part. The flanges consist of winding, pre-consolidated flange packages, multi- and angle plies. The web is made up of sandwich panels with face sheets of winding and angle plies. The corner has a multiple ply-insert and -drop configuration and a transition from a monolithic composite material to a sandwich structure. Additionally the material groups change along the length of the blade and hence results in many thousand lay-up sequences.

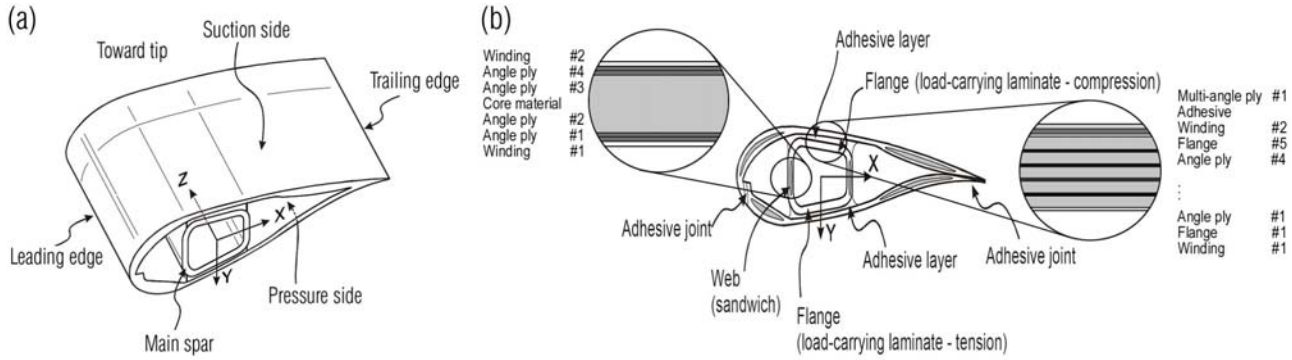

Fig. 1. The blade terminology on system level is displayed in (a) and the more detailed component level schematically presented in (b). The outcome of the many and complex lay-up sequences is thousands of material groups.

Previous parametric studies have been performed in order to predict stiffnesses correctly in regions of multiple transitions and found that the developed blade builder program will construct finite element models with at least 90% of the theoretical structural stiffness [1].

2 Applied Methods

A nonlinear fracture mechanics approach with a geometrically linear element formulation is used for analysis of a blade i.e. a finite element model with solid-shell and de-cohesive elements of the main load carrying spar. A mixed-mode geometrically nonlinear element, using a zero-thickness iso-parametric element formulation with a bilinear constitutive softening law, has been implemented in the in-house finite element program MUST [2].

The mixed-mode de-cohesive element formulation is based on the work of Camanho and co-workers [3-6]. Constitutive softening models are associated with severe solution difficulties, and therefore an efficient and robust solution strategy for dealing with large three-dimensional structures is needed and implemented. The solution strategy is based on an extended version of the approach proposed in [7].

The starting point has been a blade builder program, which is developed as a pre-processing tool for finite element models of a main spar of a wind turbine blade. In order to handle problems including damage mechanics an algorithm for handling layered cohesive elements has been implemented. The main difficulties are associated with a proper solution strategy since a node pair in a cohesive element potentially has no stiffness and the solution procedure may diverge. The cohesive element is used with a pre-implemented continuum based three-dimensional layered solid-shell element for laminated structures, with Assumed Natural Strain (ANS) interpolation in the transverse shear strain and thickness strains practically making the element locking-free and capable of shell and cohesive zone modeling [8].

A nonlinear equivalent single-layered finite shell element model has also be constructed and analyzed with regards to estimating the blade response characteristics, which is a further development from [1]. This model is also compared with the previously mentioned applied method. The model is pre- and post processed in the commercial finite element program MSC.Patran and solved with MSC.Marc.

The pre-processing of the finite element models is done with a blade builder program based on Patran Command Language and Excel spreadsheets with interpolated lay-up data for a predefined element size, which can generate blade models consisting of either shell or solid-shell elements with one element in the thickness direction. The solid-shell model is then expanded with an adaptive through-the-thickness routine that generates solid-shell elements for each laminate layer or subsection of laminate layers combined with cohesive elements at predefined interfaces.

2.1 Mixed-mode De-cohesive Formulation

Two approaches can be used to study interlaminar crack formation and propagation: The direct application of linear elastic fracture mechanics (LEFM) such as the Virtual Crack Closure Technique (VCCT) proposed by Rybicki and

Kanninen [9], the J-Integral method [10] and stiffness derivative [11]. An indirect approach can also be used, which is within the framework of damage mechanics that is based on the concept of the cohesive zone modeling. The latter is most feasible when the aim is to simulate large three-dimensional structures with propagation of multiple delamination fronts and formation of new interlaminar cracks. The cohesive zone model stems from Dugdale and Barenblatt and later Hillerborg modified it to include damage initiation. In general, the mixed-mode de-cohesive element formulation can be used for several fields within self-similar fracture, delamination, crack propagation and connections between bonded or co-cured components.

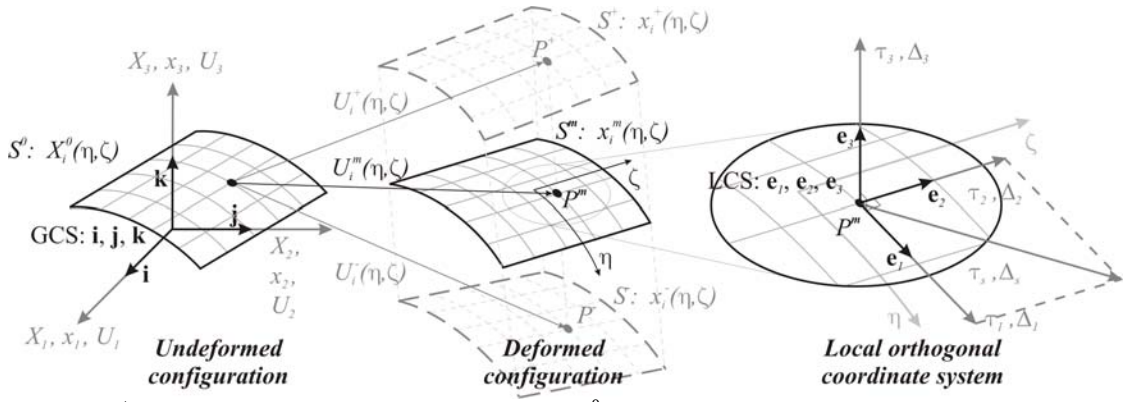

Fig. 2. The surfaces $S^{\pm}$ are coincident with the reference surface S^0 in undeformed configuration. The midpoints P^m of the line joining P^+ and P^- define the mid-surface S^m, which is defined as reference for tractions τ and relative displacements Δ.

In the indirect approach the cohesive zone model relates tractions to relative displacements. Consequently, the cohesive zone formulation is identical to Griffith's theory of fracture and the J integral proposed by Rice, since the resulting work of normal and tangential separation can be related to the critical values of energy release rates. Thus the method does not suffer from the severe mesh-sensitivity associated with softening stress/strain models or with strength-based models. Nevertheless, it still has some form of mesh sensitivity; in particular, with a coarse mesh the structural response can be very non-smooth and exhibit artificial snap-through and snap-back, since the coarse mesh can not capture the correct stress field around the delamination front as it propagates. In contrast to the direct approach, the cohesive zone model has no precisely defined crack-tip and stress singularity, but operates with a process zone and assumes self-similar delamination propagation. The present formulation is only concerned with interlaminar damage onset and propagation and does not account for intralaminar failure mechanisms.

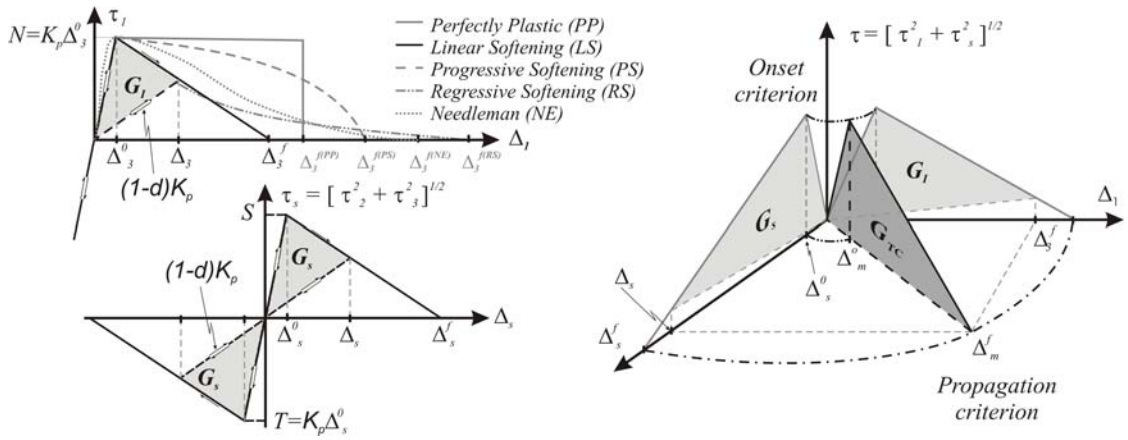

Fig. 3. The constitutive description of the de-cohesive zone model is based on a bilinear model with one damage state variable, d, in a mixed-mode propagation criterion. The superscript of the relative displacement describes the failure event (f) and the onset event (o). The subscript implying the associated local direction; the tangential norm (s), the normal direction (3) and the relative mixed-mode norm (m).

The kinematics of the de-cohesive element are described by the mid-surfaces S^m, which consist of an upper surface S^+ and lower surface S^- as shown in fig. 2. Thus the mid-surface is of zero thickness. The surfaces $S^{\pm}$ independently have rigid body motion and act with a elastic-softening response corresponding to the Mode I opening (**e**3 direction) and/or a tangential sliding (the plane spanned by **e**1 and **e**2) equal to the norm of the Mode II and Mode III of the upper and lower surface. All tractions τ_i and relative displacements Δ_i are related to the curvilinear coordinate system $x_i^m(\eta,\zeta)$ of the mid-surface. In geometric approximations the rotation dependency of global displacements is neglected which yields the possibility of neglecting geometric nonlinearities.

The mixed-mode constitutive equation, which relates the traction τ_i to the relative displacement Δ_i at the interface of two bulk materials, is shown in fig. 3. The implemented cohesive element is based on the constitutive tangent stiffness matrix.

Table 1. Material properties for unidirectional carbon fiber and polyetheretherketone matrix used in benchmarks

Elastic properties for lamina, t = 1.56mm					
E_{11} MPa	$E_{22}=E_{33}$ MPa	$G_{12}=G_{13}$ MPa	G_{23} MPa	$\nu_{12}=\nu_{13}$	ν_{23}
122.7	10.1	5.5	3.7	0.25	0.45
Fracture material properties for lamina					
G_{IC} J/m^2	G_{IIC} J/m^2	T MPa	S MPa	K N/mm	μ
0.969	1.719	80	100	10^6	2.284
Model properties					
Length (l) mm	Width (b) mm	Thickness(t) mm	Ini. crack mm	Mesh lxbxt	
102.0	25.4	3.12		150x1x3	

One characteristic of all softening models is that the cohesive zone still can transfer load after the onset of damage, see fig. 3(left). For pure mode loading the area under the traction-relative displacement curve is the mode I and tangential mode fracture energies, G_I and G_S, respectively. G_{IC} is the total critical energy release rate for mixed-mode propagation criteria, which correspond to a mixed-mode relative displacement at failure Δ^f_m in fig. 3(right). The relative mixed-mode displacement norm $\Delta_m = [\langle\Delta_3\rangle^2 + \Delta_s^2]^{1/2}$ and $\Delta_s = [\Delta_1^2 + \Delta_2^2]^{1/2}$ is associated with the relative pure-mode displacements Δ_i, where $\langle x\rangle$ is the McCauley operator, $\langle x\rangle = \frac{1}{2}[x + |x|]$, which emphasizes that the normal compressive relative displacement do not contribute to the relative mixed-mode displacement norm i.e. to the damage onset or propagation.

A power-law (PL) failure criterion based on interlaminar tractions has been used to predict onset of delamination [12] and to simulate the progression of delamination under mixed-mode loading the PL criterion is reformulated in energy release rates and fracture toughnesses. The more recently proposed Benzeggagh-Kenanes (BK) criterion [13] is also implemented for onset and propagation. Dávila and Camanho developed a bilinear constitutive law, fig. 3(left), that can be used with any mixed-mode failure criterion, fig. 3(right) [4]. In order to assure a smooth transition from the initial damage surface to the propagation surface as proposed by Turon et. al. [14] the delamination onset and propagation criteria are interlinked.

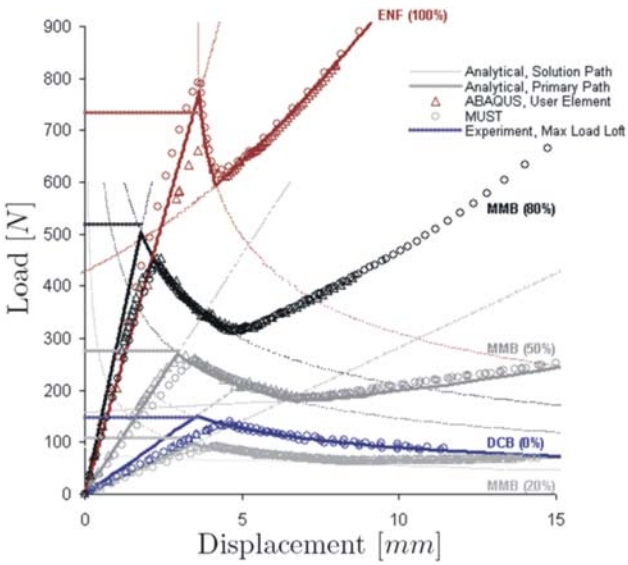

Fig. 4. Benchmark of implemented de-cohesive element, analytical solution, experimental values and ABAQUS user-defined element results.

The implementation of the de-cohesive element formulation is verified in fig. 4 by comparing results from analytical solutions given by [15] and experimental values taken from [4] for the Double Cantilever Beam (DCB), Mixed-Mode Bending (MMB) and End-Notched Flexure (ENF) test specimen. The material properties and geometric properties of the test specimens are listed in table 1. The results in fig. 4 show the load as a function of the center deflection of the test specimens with mode II and the end deflection for pure mode I test specimen. The differences in the initial stiffness response stems from the boundary assumption for the analytical beam models, which are assumed to be

fixed whereas the finite element models are flexible supported at the end with no damage. The degree of mode-mixity β is defined below and is given in parentheses after the name definition on the graphs in fig. 4.

$$\beta = \frac{\Delta_s}{\langle \Delta_3 \rangle + \Delta_s} \qquad (1)$$

2.2 Solution Strategy with Subplane Control

A full Newton method must be used in order to achieve convergence. When using a global solution approach it is convenient to use a line search algorithm and in case of convergence difficulties, many iterations using the secant stiffness matrix can be beneficial. However global methods, in the case of damage analysis with highly localized deformations, have proven to be ineffective.

Considering the dominant Degrees Of Freedom (DOF) initially suggested by De Borst [16] in the updated normal plane method gives an indirect displacement control i.e. the subplane control approach. In more general terms the control vector or matrix consists of scalar functions for the dominant DOF chosen at each increment as proposed by Geers [17-18].

Code implementation experience has shown the apparent best method, for the implemented cohesive element, to be an extended version of the proposed approach by Crisfield and Alfano [7]. This subplane control consists of a control vector, with components that are linear local-control functions chosen in each increment in such a way that the control function monotonically increases in the loading direction for further damage propagation.

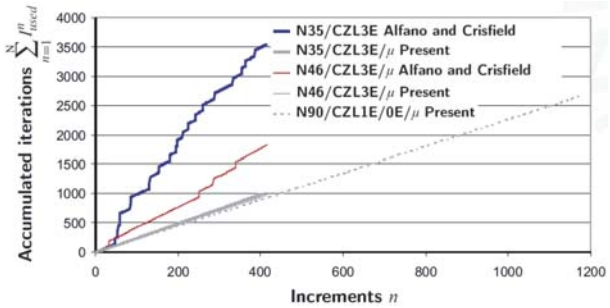

Fig. 5. Incremental history for minimum CZL in a DCB test specimen model with different solution strategies.

Additionally, viscous regularization can be used to improve the convergence rate when having small cohesive zones. The viscous regularization delays the damage uptake in the structure and may increase the convergence rate [19].

The labels in figs. 5 and 6 are denoted such that the number succeeding N is the maximum possible value of the allowable traction in the normal direction, see N on fig 3(left), with the given model mesh density without divergence. The number after the Cohesive Zone Length (CZL) specifies the minimum number of elements in the CZL at any given point during the analysis. μ indicates the use of viscous regularization. All things considered; the higher value of N, the smaller CZL, which results in the need for more solver-robustness. Each vertical step in the iteration history corresponds to a load step cutback. When using viscous regularization one can reduce the number of cutbacks. Additionally when using the present solver strategy, see fig. 5, no cutbacks are introduced and each increment convergences in two to three iterations regardless of stable or unstable propagation, see [20] for further information on the implemented solution strategy.

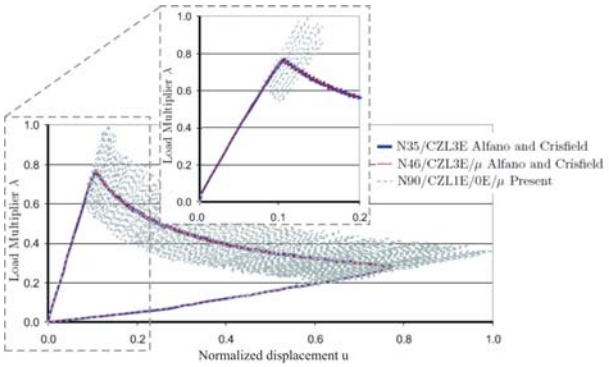

Fig. 6. DCB test specimen response of solution strategies with minimum obtainable CZL, correspond to fig. 5.

It is evident that the present solution strategy is the most robust and efficient of the methods shown. Since the present solution strategy merely is an extension of [7] it obtains the same results with the same choice of the allowable normal traction N. The obtained solver robustness and efficiency with regard to a coarse mesh in the cohesive zone has a prize in loss of accuracy in the structural load response. In the case of the DCB test specimen with N90 the cohesive zone is only represented by one element in every second increment i.e. in one increment one element carries the cohesive forces and in the next no element do. This gives many large

artificial cutbacks shown on fig. 6. Nevertheless the loss in accurate structural response characteristics compared to gain in solver robustness and efficiency is a necessity when solving large three-dimensional structures.

Even though the solution strategy performs well in the benchmark problems given above, where it is affordable to have a relative fine mesh, only one and in some cases two delamination fronts and small load steps, other complications arise in the case of large three-dimensional structures, especially when traversing material instability points with propagation of multiple delamination fronts and formation of new interlaminar cracks. In order to overcome some of these issues, an alternative cutback procedure is used.

In the alternative cutback procedure the solver uses the constitutive secant stiffness matrix a maximum of two times in a row. Subsequently, the solver is forced to unload the structure and find an equilibrium point with the constitutive tangent stiffness matrix. This ensures that the structural response corresponds to the primary equilibrium path. If the solution strategy uses the constitutive secant stiffness matrix together with viscous regularization and later uses the constitutive tangent stiffness matrix then it will, in most cases, not achieve convergence ever again. The structure will then follow an equilibrium branch that is not the true structural response characteristic. Equilibrium on the primary equilibrium path can only be achieved again if this equilibrium branch intersects or is in a close neighborhood of the primary equilibrium path. Implementation experience has shown that this is best achieved by forcing unloading after using the constitutive secant stiffness matrix to traverse a material instability point.

3 Wind Turbine Blade

A wind turbine blade is investigated based on full scale experiments, a geometrically nonlinear finite element analysis and the implemented nonlinear fracture mechanics formulation and solution strategy.

Two loads are defined which are the first failure load and the collapse load. All finite element models are analyzed according to 125% of the first failure load.

2.3 Geometrically Nonlinear Analysis

The geometrically nonlinear analysis is based on an equivalent single layered shell element model of a complete main spar, see fig. 9. The model consists of 7.260 nodes, 7.200 elements, 574 real constant sets (lay-up sequences) and 5 linear elastic base materials.

Two models are investigated, namely an idealized model and a model with an imposed optimum initial geometric imperfection amplitude based on the measured strain field from the test case. The optimum geometric imperfection amplitude is determined by imposing a geometric imperfection field based on the strain gauge measurements and then minimizing the differences between the test results and a geometrically nonlinear analysis of the blade.

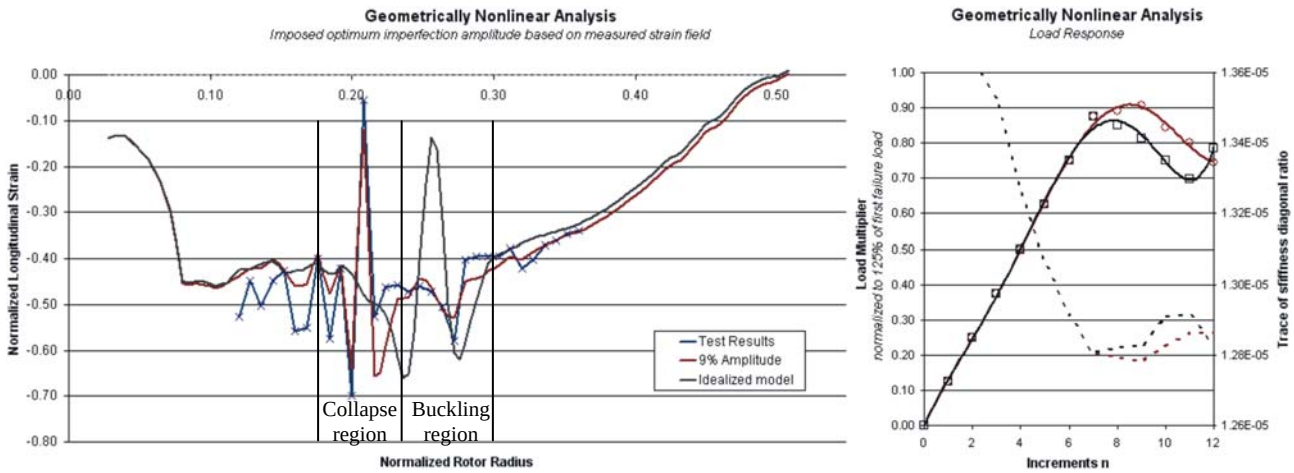

Fig. 8. Results of geometrically nonlinear analysis for an idealized model and a model with a imposed optimum imperfection amplitude based on the measured strain field.

The amplitude was found to be 9% normalized according to flange thickness. This has previously been done in a linearized prebuckling setting and the optimum imperfection was found to be 22% [1]. The smaller imperfection amplitude found in the geometrically nonlinear setup is more plausible.

The structural response in fig. 8(left) is the normalized longitudinal strain field on the compression side of the blade. Two regions are of interest, namely the region with maximum strain, which is where the blade suffers a total structural collapse and the buckling critical region. The collapse region is triggered by an initial geometrical imperfection and the buckling region is triggered by material transitions in the blade. These instability phenomena will with great plausibility interact if they occur at the same load level. Even though they do not transpire at the same load level, delamination propagation can still trigger buckling, by decreasing the local moment of inertia at the boundaries of the buckling critical region. Hence lowering the critical buckling load in such a manner that they will occur at the same load level.

The critical buckling loads are calculated as 1.00 and 1.04 normalized according to the collapse load for the idealized model and the 9% amplitude model, respectively. The critical load level in the imperfect blade actually increases because the imperfection field prevents the buckling mode found in the idealized model. The strain level found at the buckling critical region in the imperfect blade is much lower than the strain level determined by the idealized model, which correspond well with full scale experiment. Thus in this case the occurrence of buckling is very difficult to determine with the given measurement technique.

2.3 NLFM Analysis

In order to have a finite element model of a reasonable structural size in NLFM analysis and still have a relative fine element mesh it is chosen to model a corner of the main load-carrying spar. Not the complete model is used but a section that contains the buckling and collapse region, see fig. 8. The model is restricted to a symmetrical boundary condition in the YZ-plane at the compression flange and an anti-symmetrical boundary condition in the XZ-plane at the webs, see fig. 9. The model consists of 23.370 nodes, 19656 elements, 660 real constant sets (lay-up sequences), 5 linear elastic base materials and 1 fracture mechanic property set. The model is made up of 5 cohesive zones with layered solid-shell elements in between.

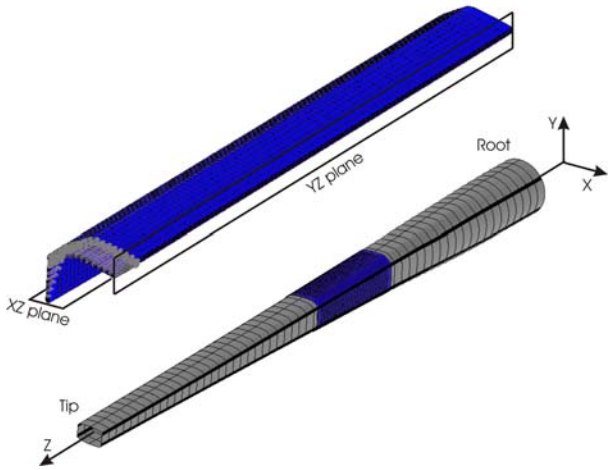

Fig. 9. The critical buckling and collapse region of the main spar is shown on the complete shell model together with the reduced solid-shell/cohesive model.

A post-mortem analysis of the collapsed blade section has shown that the fracture processes primarily initiate and propagate in the angle plies between the pre-consolidated flange packages and core material. The delaminations in the angle plies are found to propagate into very large portions of the structure. The collapsed zone is almost a fracture line of crushed laminae i.e intralaminar damages. The crushed laminae are localized though. Therefore in order to model the main fracture energy uptake in the structure it is chosen to model 5 cohesive zones through the length of the blade where the delamination is seen to propagate in the post-mortem analysis. No intralaminar damage models are used i.e. the energy uptake at the localized intralaminar fracture line is not accounted for, but the main interlaminar fracture energy is used in the interlaminar crack formation and delamination progression, which is modeled by the de-cohesive element. The solution is done in a geometrically linear setting, so no interaction between geometric and material instability will be accounted for.

The blade is fixed at the end toward the root and loaded with 125% of the first failure flap-wise test load at the opposite end. This corresponds to a cantilever beam subjected to a bending moment and a shear force in the flap-wise direction. At the ends of the spar a row of elements act as a load

introduction region, where no damage can be initiated and propagate.

Fig. 10 displays the results of the layered cohesive zone procedure in a region where multiple layered cohesive elements have been detected. The attributes of these elements are reassigned so that damage only can propagate in strategically chosen elements in this region. Benchmarks of simple DCB test specimen with multiple layered cohesive elements have been performed, but are not shown within the paper. The results are that the structural response is identical to that of a DCB test specimen with one cohesive zone, see fig. 6, nevertheless the convergence rate is strongly dependent on the number of layered cohesive elements.

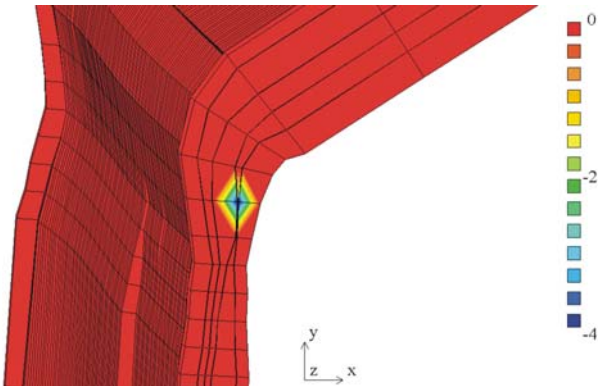

Fig. 10. Detection of layered cohesive elements and reassigning element attributes. A node value of -2 indicates a double layered cohesive element and -4 indicates a multiple layered element.

The response characteristic of the blade is very non-smooth due to the coarse mesh in the model, see fig. 11. The last load increment before traversing the material instability point is determined to be 1.03 normalized according to the measured collapse load at which the blade suffered a total progressive collapse. The average load capacity of the finite element model after the material instability point is calculated as 0.90 with a 0.16 average bound of the load peaks normalized according to the collapse load.

The response is very non-smooth and exhibit artificial snap-through and snap-back, since the coarse mesh can not capture the correct stress field around the delamination fronts as it propagates. Besides the difficulties in achieving convergence of the solution the critical load is not given clearly in the response characteristic. To remedy this one has to have a higher mesh density.

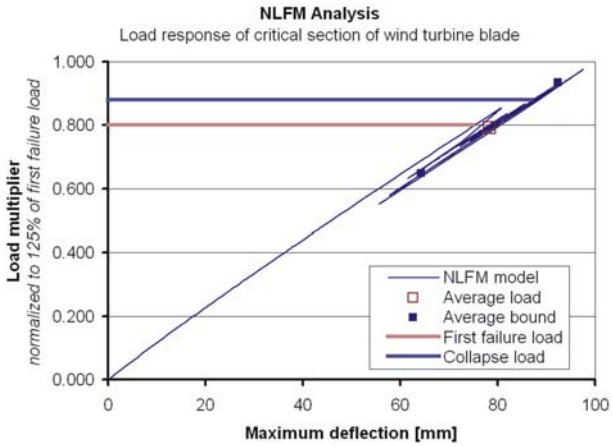

Fig. 11. Structural response of the wind turbine blade section in the NLFM analysis. The model is subjected to 125% of the first failure load during test.

Generally the solution convergences within one to three iterations per increment, but due to the coarse mesh cutbacks are unfortunately not avoided. Fig. 12 shows the accumulated nodal damage as a function of increments. The damage uptake until increment 211 is stable delamination onset and propagation whereas the remaining unstable delamination onset and propagation is after the traversing of the material instability point. The percentage of viscous damping in each increment is also displayed in fig. 12 and the amount of damped energy is very small i.e. it has no effect on the structural response of the wind turbine blade.

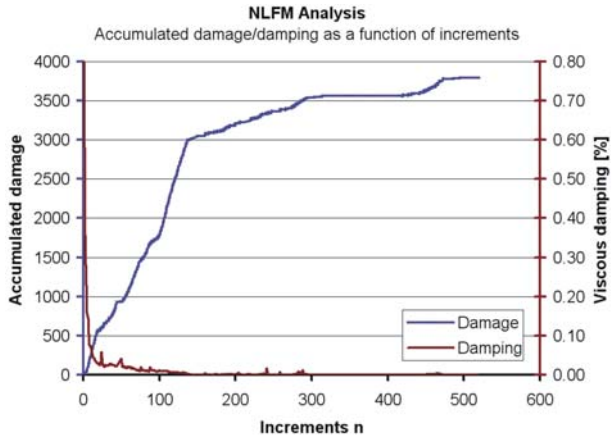

Fig. 12. Incremental history of the accumulated damage and viscous damping.

4 Discussion

The developed blade builder program and the geometrically nonlinear models perform well in prediction of the critical buckling load, see fig. 8 and table 2. Nevertheless the imposed geometrical

imperfection increases the buckling load. On the actual blade a geometrical imperfection would not increase the critical buckling load instead it would decrease the critical load due to a local bending boundary layer resulting in a premature damage initiation and propagation.

The implemented mixed-mode de-cohesive element formulation and the present subplane solution strategy perform very well in simple benchmark cases, see figs. 4-6. Moreover the present solution strategy makes it possible to solve large three-dimensional models like the section of the wind turbine blade. In the case of the wind turbine blade section the very non-smooth structural response compromises a clear statement of the material instability point and nature of the unstable delamination path. Nevertheless the deducted values from the NLFM analysis correspond very well with the actual flap-wise collapse load, see table 2.

Table 2. Critical loads of wind turbine blade

Geometrically nonlinear model Normalized load with respect to the collapse load, full scale test		
Idealized model	1.00	
9% imperfection model	1.04	
Nonlinear fracture mechanics model Normalized load with respect to the collapse load, full scale test		
Model / 5 cohesive zones, Material instability point	1.03	
Model / 5 cohesive zones, start of unstable delamination	0.90	±0.16

The geometric and material instability points are almost coinciding, which is a strong indication that they will interact and indeed cause a progressive collapse of the wind turbine blade as seen in the full scale experiment.

Unfortunately it has not been possible to investigate the interaction between the geometric and material instability phenomena. This will be a topic for the future. First a linearized prebuckling behavior in a NLFM framework will be investigated, although linearized prebuckling is strictly applicable to conservatively loaded systems, which is not the case with NLFM analysis. Consequently the calculated critical load multiplier from the current damage and deformation configuration will be an estimate for an equivalent conservatively loaded system with damage but no damage propagation. Hereby the influence of damage propagation on the critical load multiplier can be found, but not vice versa. In the future the aim is also to predict full interaction, when solving the geometrically nonlinear and NLFM analyses simultaneously. This is computationally costly and requires further development of the solution strategy.

References

[1] L.C.T. Overgaard, E. Lund. ”Structural design sensitivity analysis and optimization of Vestas V52 wind turbine blade”. In: *Proc. WCSMO6 - 6th World Congress on Structural and Multidisciplinary Optimization* (Eds. J. Herskovits, S. Mazorche and A. Canelas), 30 May - 3 June 2005, Rio de Janeiro, Brasil, CD-ROM, ISBN: 85–285–0070-5, 10 pages.

[2] MUST. The MUltidisciplinary Synthesis Tool. *Aalborg University*, http://www.ime.aau.dk/MUST/.

[3] P.P. Camanho, C.G. Dávila. “Numerical simulation of delamination growth in composite materials”. *NASA/TR-2001-211041*, August 2001.

[4] P.P. Camanho, C.G. Dávila. “Mixed-mode decohesion finite elements for the simulation of delamination in composite materials”. *NASA/TM-2002-211737*, June 2002.

[5] P.P. Camanho, C.G. Dávila, M.F. de Moura. “Numerical simulation of mixed-mode progressive delamination in composite materials” *Journal of Composite Materials*, 37 (16), pp. 1415-1438, 2003.

[6] A. Turon, P.P. Camanho, J. Costa, C.G. Dávila. “An interface damage model for the simulation of delamination under variable-mode ratio in compositematerials”. *NASA/TM–2004–213277*, October 2004.

[7] G. Alfano, M.A. Crisfeld. “Solution strategies for the delamination analysis based on a combination of local-control arc-length and line searches” *International Journal for Numerical Methods in Engineering*, 58, pp. 999-1048, 2003.

[8] L. S. Johansen, E. Lund- “Optimization of geometrically linear/nonlinear laminated composites through delamination criterion and model adaptivity”. In: *Proc. WCSMO7 - 7th World Congress on Structural and Multidisciplinary Optimization*, 21 – 25 May 2007, Seoul, Korea, CD-ROM, 10 pages.

[9] Rybicki, E., M.F. Kanninen. “A finite element calculation of stress intensity factors by a modified crack closure integral”. *Engineering Fracture Mechanics* 9 (1977), pp. 931–938.

[10] Rice, J. “A path independent integral and the approximate analysis of strain concentration by notches and cracks”. *Journal of Applied Mechanics* 35 (1968), pp. 379–386.

[11] Parks, D. “A stiffness derivative finite element technique for determination of crack tip stress intensity factors”. *International Journal of Fracture* 10(4) (1974), pp. 487–502.

[12] Ye, L. “Role of matrix resin in delamination onset and growth in composite laminates”. *Composites Science and Technology*, 33(4) (1988), pp. 257–277.

[13] Benzeggagh, M., Kenane, M. “Measurement of mixed-mode delamination fracture toughness of unidirectional glass/epoxy composites with mixed-mode bending apparatus”. *Composites Science and Technology* 56 (1996), pp. 439–449.

[14] Turon A., P.P. Camanho, J. C., Dávila, C. “An interface damage model for the simulation of delamination under variable-mode ratio in composite materials”. *NASA/ TM–2004–213277*, October, 2004.

[15] Mi, Y., Crisfield, M. “Analytical derivation of load/displacement relationship for the DCB and MMB and proof of the FEA formulation”. *Department of Aeronautics*, Imperial College, April, 1996.

[16] Borst, R. D. “Computation of post-bifurcation and post-failure behaviour of strain-softening solids”. *Computers & Structures*, 25 (1987), pp. 211–224.

[17] Geers, M. “Enhanced solution control for physically and geometrically non-linear problems. Part i - the subplane control approach”. *International Journal for Numerical Methods in Engineering*, 46 (1999), pp. 177–204.

[18] Geers, M. “Enhanced solution control for physically and geometrically non-linear problems. Part ii - comparative performance analysis”. *International Journal for Numerical Methods in Engineering*, 46 (1999), pp. 205–230.

[19] Abaqus Inc., ABAQUS 6.5 User's Manual, Pawtucket, U.S.A., 2005.

[20] L.C.T Overgaard, E. Lund. “Structural instability phenomena in wind turbine blades”. In: *2nd PhD Seminar on Wind Energy in Europe*, Risoe National Laboratory, 2006, 8 pages.

[21] A. Turon, C.G. Dávila, P. C., Costa, J. “An engineering solution for using coarse meshes in the simulation of delamination with cohesive zone models”. *NASA/ TM–2005–213547*, March, 2005.